Nanomaterials and Nanotechnology

OPEN ACCESS
ARTICLE

Wrinkling Behaviour of Annular Graphynes under Circular Shearing Load Using Molecular Dynamics Simulations

Regular Paper

Yanling Tian[1], Zheng Li[1*] and Kunhai Cai[1]

1 Key Laboratory of Mechanism Theory and Equipment Design of Ministry of Education, Tianjin University, Tianjin, China
* Corresponding author(s) E-mail: lizhengctr@tju.edu.cn

Received 07 October 2014; Accepted 26 February 2015

DOI: 10.5772/60461

Abstract

Graphyne, a novel carbon allotrope, is a two-dimensional lattice of sp^2+sp^1 hybridization-type carbon atoms, similar to graphene. The initiation and development of wrinkles in single-layer graphynes (α-, β-, γ-, and 6, 6, 12-graphyne) subjected to in-plane circular shearing are investigated. In comparison with graphene, wrinkle pattern and profile characterization in relation to wave number, wavelength and amplitude of graphynes are extensively explored using classic molecular-dynamics (MD) simulations. Unlike graphene, the wave numbers of graphynes increase with increasing rotational angles; the wavelengths reduce correspondingly. The amplitudes show an increasing trend, with some local drops when the rotational angles increase. The drops occur as the positions of the wave numbers increase. Graphynes have superior fracture properties to graphene, despite the densities of graphynes being far lower. The fracture rotational angles depend on the percentages of acetylenic linkages in the graphyne structures: the more acetylenic linkages, the larger the fracture rotational angles. Meanwhile, acetylenic linkages also affect the bond length strains of the graphynes during the wrinkling process. The influences of the temperature on the fracture rotational angles are also examined to obtain further insights into the mechanical properties of such kinds of carbon allotropes. The achieved results can be used as guidelines for the wrinkling control and potential applications of graphynes.

Keywords graphyne, circular shearing, wrinkling pattern, acetylenic linkage

1. Introduction

Due to its excellent mechanical, thermal and electronic properties, graphene has attracted tremendous research attention in recent years [1, 2]. Extensive research efforts have been devoted to exploring the unique characteristics and potential applications of such kinds of single-layer carbon nanostructures [3, 4]. Like fullerenes and carbon nanotubes, graphenes are considered as an sp^2-hybridized carbon material. However, the versatile flexibility of carbon makes it possible to form three types of hybridization state (sp^3, sp^2 and sp^1). Thus, it is feasible to design a number of combinations to form different carbon allotropes. Mixed sp^2 and sp^1 hybridization was first proposed by Baughman et al. [5] in 1987. Graphyne and some macrocyclic subunits capable of forming this kind of single-layer carbon allotrope were discussed. Ten years later, the graphdiyne of the

same group of (sp^2+sp^1) allotropes was designed by Haley et al. [6] in 1997. Theoretical predictions and analyses have been extensively conducted and a series of useful results have been obtained. The proposed subunits, including perethynlated dehydroannulenes, expanded radialenes, radiaanulenes with large, expanded "Platonic" objects, and alleno-acetylenic macrocycles, will in the near future be available to serve as precursors for graphyne and graphdiyne [7]. However, the experimental synthesis of such kinds of carbon allotrope made little progress until the thin film of graphdiyne was successfully synthesized on a copper substrate by a cross-coupling reaction using hexaethynylbenzene in 2008 [8]. Further experimental synthesis of graphyne and graphdiyne can be expected, and potential applications of such kinds of carbon allotropes in polymer solar cells, photocatalysts, and electrics are already being explored [9-11].

Recent research efforts have also been directed towards the characterizations of these kinds of carbon allotropes [12-16]. Cranford et al. [17] utilized classical molecular dynamics (MD) with ReaxFF force field to explore the adhesion energy, effective sheet thickness, Young's modulus and out-of-plane bending stiffness. Their results showed that graphynes have superior performance to graphene in many aspects, especially in terms of electronic properties. Salmalian et al. [18] studied the buckling of graphynes using molecular-dynamics simulations. They observed that zigzag graphynes have larger buckling forces than armchair graphynes, and that sheets with more acetylenic linkages had smaller critical compressive forces. Shao et al. [19] explored the temperature-dependent mechanical properties including Young's modulus and strength of graphyne using a first-principle calculation combined with quasi-harmonic approximation. They noted that increased temperature was able to reduce the mechanical properties of graphyne. Zhang et al. [20] investigated the effects of hydrogenation on the mechanical properties of graphynes using the MD simulations. They found that location, distribution and coverage of hydrogenation had significant effects on Young's modulus, fracture stress and fracture strain. Majidi et al. [21] investigated the effects of formaldehyde on graphyne based on the density functional theory (DFT). Here, graphynes showed a semiconducting property in the presence of formaldehyde, and the high-sensitivity sensors used for the detection of formaldehyde could be searched using the graphyne material.

Wrinkling is a ubiquitous characteristic of ultra-thin films. It has been demonstrated that wrinkles in graphene usually lead to some remarkable physical properties and great potential for application in scientific and engineering fields [22-27]. Much research effort has been dedicated to the wrinkling behaviour of graphene in recent years. However, few studies have focused on the wrinkling properties of graphynes, which may suggest further potential applications due to the special topographies of this kind of carbon allotropes. This paper therefore seeks to fill this research gap. The wrinkling behaviours of annular graphynes under circular shearing load are explored using MD simulations. The paper is organized as follows. In Section 2, we introduce the simulation models and methodology in detail. Section 3 is devoted to the description of wrinkling morphology and variations of the wrinkling pattern. Further, the average energy and failure torque are investigated to obtain deep insights into the mechanical properties of graphynes. In particular, comparisons between graphynes and graphene are conducted to explore the roles that acetylenic linkages play in hexagonal ring structure. Finally, conclusions are provided in Section 4.

2. Simulation model and methodology

In this paper, four kinds of graphynes (α-, β-, γ-, and 6, 6, 12-graphynes), as well as graphene (shown in Fig. 1) are adopted to investigate the wrinkling behaviour of such kinds of monolayer carbon allotropes. These graphynes differ from one another in the percentage of acetylenic linkages in their atomic structures (see Table 1). It has been validated that the presence of acetylenic linkages in graphynes can affect many of their mechanical properties, including Young's modulus, fracture strain, and fracture stress [28].

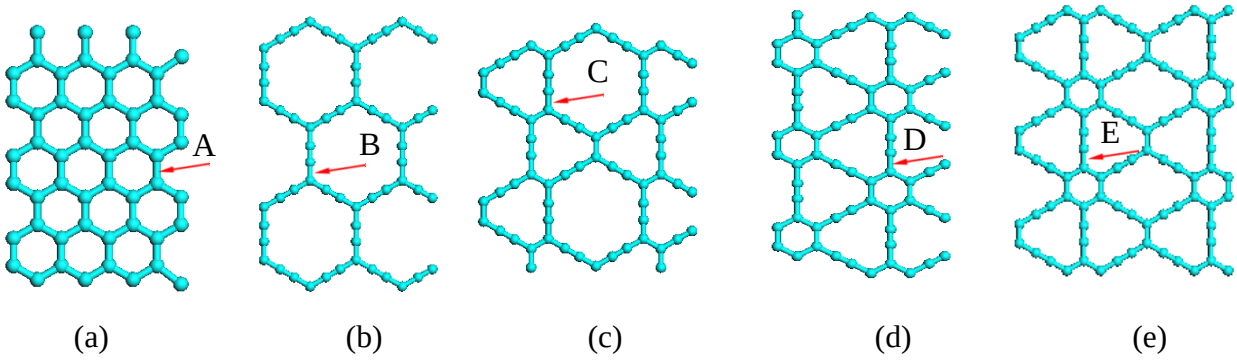

Figure 1. Atomistic models of graphene and four different graphynes: (a) graphene; (b) α-graphyne; (c) β-graphyne; (d) γ-graphyne; (e) 6, 6, 12-graphyne

Carbon allotropes	α -graphyne	β -graphyne	6, 6, 12 -graphyne	γ -graphyne	graphene
Acetylenic linkages (%)	100	66.67	41.67	33.33	0

Table 1. Percentage of acetylenic linkages of graphynes and graphene sheets

A succession of MD simulations of wrinkling behaviour of graphynes was performed, using the open-source software LAMMPS to conduct computational analyses. The annular graphynes' sheets were utilized to explore the wrinkling properties under circular shearing strain. The outer radius r_o of the annular graphynes was fixed at 9 nm, and three different outer-to-inner radius ratios (r_o/r_i= 2:1, 3:1, 4:1) were utilized. The graphynes and graphene simulation models are shown in Fig. 2, where the outer-to-inner radius ratio is 3:1. The maximum angular periodicities of graphene and α-, β-, and γ-graphynes are both 60°, while that of 6, 6, 12-graphyne is 90°. The boundary conditions of the simulations were selected as follows: the blue portion labelled as "outer" is fixed completely and all DOFs (Degrees of Freedom) of the atoms are set to zero; the red portion labelled as "inner" rotates at a constant speed, ω, anti-clockwise; the green portion labelled as "mobile" is free of constraint. The interactions between carbon atoms are described using AIREBO potential [29-31], which has been successfully utilized previously to analyse the mechanical and thermal properties of carbon-based nanomaterials, including carbon nanotubes and graphene [32, 33]. The AIREBO potential is capable of breaking and forming covalent bonds with associated changes in atomic hybridization, and thus it provides a powerful method for modelling complex chemistry in carbon-based nanosystems. In order to avoid the violent increase in the tensile force when C-C bonds are stretched beyond 1.7 Å, the maximal cut-off parameter of the AIREBO potential was set as 2.0 Å [20, 28, 34]. The atomic models were firstly optimized to minimize the potential energy of each entire system. The energy minimization tolerances were chosen as 10^{-12} eV. Based on the obtained stable models, extensive MD simulations were conducted using the NVT (constant number, volume, and temperature) ensemble and the Nose-Hoover thermostat algorithm [35]. The temperature was kept constant at 1 K to reduce the influence of thermal vibrations. The Velocity-Verlet [36, 37] time-stepping method was employed and the integration time step set as 0.001 ps. The loading angular speed of the inner section was chosen as ω = 0.01 degree/ps.

3. Results and discussions

The graphynes and graphene sheets with different outer-to-inner radius ratios show similar initial and development wrinkling characteristics. For simplification, we take α-graphyne with outer-to-inner radius ratio approximately equal to 3 as an example to explore the wrinkling process, where the rotation angle θ is increased from 0° to 20°. The influences of the geometric parameter, i.e., the outer-to-inner radius ratio, on the wrinkling behaviour is discussed

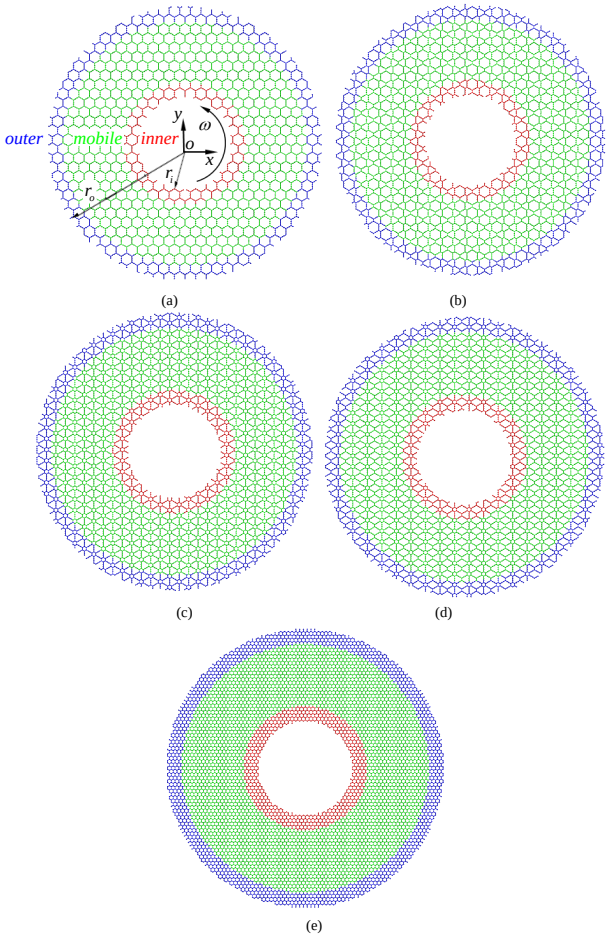

Figure 2. Simulation diagrammatic sketch of annular graphyne and graphene sheets: (a) α-graphyne (4037 atoms); (b) β-graphyne (5251 atoms); (c) γ-graphyne (6181 atoms); (d) 6, 6, 12-graphyne (6314 atoms); (e) graphene (8752 atoms)

in detail in section 3.2. It is observed that the annular α-graphyne sheet remains flat initially, before the rotation angle is increased to 0.68° (initial wrinkling angle). When the in-plane shearing strain exceeds the initial wrinkling angle, wrinkles are generated on the annular sheet. Unlike the wrinkle development on the rectangular graphene sheet under in-plane shearing strain [24], there is no obvious wrinkle development in these studies. The wrinkles suddenly appear throughout the annular sheet, mainly due to the fixed constraint conditions on the inner and outer sides. When the circular in-plane shearing strain reaches 11.7° (fracture rotational angle), the carbon-carbon bond breaks and the annular sheet enters the fracture process.

3.1 Wrinkle pattern

For simplicity without loss of generality, the annular α-graphyne sheet under a rotation angle of 6° was chosen to investigate the wrinkling patterns without carbon bond breaking. The wrinkling contour is shown in Fig. 3(a); the circumferential section at the maximum wrinkle crest, i.e., radius of 4.5 nm, is shown by the broken circular lines

labelled as "*L*". The wrinkling profiles are shown as sinusoidal forms plotted in Figs. 3(b) and (c). Considering the non-smooth inner boundary, each wrinkle is similar to another but has different geometrical scales, and the wave crest is an approximate mirror image of the wave trough; thus, the wave crest was utilized to study the variation of the wrinkling pattern. In order to show individual wrinkles intuitively, a typical wrinkle labelled as "*leaf*" was extracted, as shown in Fig. 3(a), with the corresponding shape in the longitudinal direction (the direction along η) plotted in Fig. 3(d) and the amplitude normalized by the maximum out-of-plane displacement (labelled as "*top*" in Fig. 3(d)). The wrinkling pattern is related to the bending energy and stretching energy stored in the graphynes and graphene. The closer the sections are to the inner radius, the higher their bending energy, as a result of their prominent curvature. The wrinkling pattern presents decay along the longitudinal direction and indicates a transition from bending to stretching. Hence, from the shape of each wrinkle there is an interchange of bending energy and stretching energy, which is in good agreement with previous research results obtained for annular graphene [38, 39].

3.2 Wrinkle profile

The wrinkling pattern can be characterized by the wave number, wavelength and amplitude. In this framework the differences in wrinkling pattern between graphene and graphynes were analysed. It was found that the wave numbers of graphene remain constant, i.e., 9, from the wrinkling initiation to the first bond breaking, which is consistent with previous research [38]. It must be pointed out that the ratios of outer-to-inner radius can affect the wave number. The wave numbers change to 10 for radius ratio 2:1, and 6 for radius ratio 4:1. The wave numbers of graphene remain constant for the specified radius ratios, but, on the contrary, the wave numbers of graphynes with the radius ratio 3:1 show an increasing trend with increasing shearing load, as shown in Fig. 4. It can be seen that the α-graphyne has the smallest initial wave number of 4, while the others have the wave number 5. With increasing shearing load, the wave numbers increase correspondingly. However, the increases are not linear and smooth. The wave number curves generally suddenly jump to a value and remain constant for a while, repeating this procedure until the maximum wave numbers are reached during the wrinkling process. This behaviour is totally different to that of graphene, although the influences of the radius ratio on the initial wave numbers are similar. That is to say, increases in outer-to-inner radius ratios reduce the initial wave numbers of the graphynes. The reason for these changes in wave numbers with the graphynes may lie in that fact that mixed sp^2 and sp^1 hybridization leads to lower bond strength and out-of plane stiffness than sp^2 hybridization. For the specified radius ratio 3:1, the maximum wave number of α-graphyne is the same as that of graphene. β-graphyne has the smallest maximum wave number, 7. γ- and 6, 6, 12-graphynes have a maximum wave number of 8. It can also be seen that the initial wrinkling angle of graphene is larger than those of the graphynes. α-graphyne has the smallest initial wrinkling angle; the other graphynes have almost the same initial wrinkling angles, between those of graphene and α-graphyne. It must be pointed out that the maximum wave number remains constant with increasing circular in-plane shearing load. For a specific annular sheet, the wave numbers are inversely proportional to the wavelengths. Thus, the wavelengths, λ, of such kinds of carbon allotropes demonstrate a trend in opposition to that of the wave numbers, as shown in Fig. 5 (a). The final wavelengths of graphene and α-graphyne are both approximately 3.12 nm, measured at the *L* circumferential section. β-graphyne has the largest final wavelength of 4.0 nm; those of γ- and 6, 6, 12-graphynes are both 3.5 nm. Fig. 5(b) shows the wrinkling amplitude changes in relation to the circular shearing load. It can be seen that the wrinkling amplitudes of graphene linearly increase approximately from 0.08 nm to 0.26 nm, with rotational angles increasing from 1.9° to 7.2°. However, the graphynes show increasing trends with some local drops. In general, the rates of increase for the graphynes are lower than for graphene. Comparing the change in wave numbers with that in amplitude, we can see that the wrinkling amplitudes drop at the point where the wave numbers increase. This is because the topography reconstruction changes the potential energy distribution of the carbon allotropes. When the wave numbers remain constant, the wrinkling amplitudes of graphynes also approximately linearly increase in relation to the rotational angles. However, due to the non-continuous changes in the dihedral angle in the adjacent hexagonal ring, the amplitudes of graphynes and graphene do not strictly increase with the rotational angles. In order to obtain further insights into the properties of such kinds of carbon allotropes, the relationship between percentages of acetylenic linkages and the initial wrinkling angles, as well as wrinkling amplitudes, was explored. It was observed that the more acetylenic linkages there are, the smaller the initial wrinkling angle (α=0.68, β=0.97, 6, 6, 12=1.12, γ=1.31, graphene=1.8). Although there are some abnormal points, we can still conclude that the more acetylenic linkages there are, the larger the wrinkling amplitudes. We can also see that α-graphyne is the softest material, which is in agreement with the research conducted by Ducere et al. [40].

3.3 Energy and torque

In order to further investigate the mechanical properties of the graphynes and graphene, the average potential energy and resultant torque were recorded during the computational analyses. The obtained results are shown in Fig. 6. We can see that the average potential energy quadratically increases with the increasing rotational angles until the fracture points. After the fracture points, the energy curves

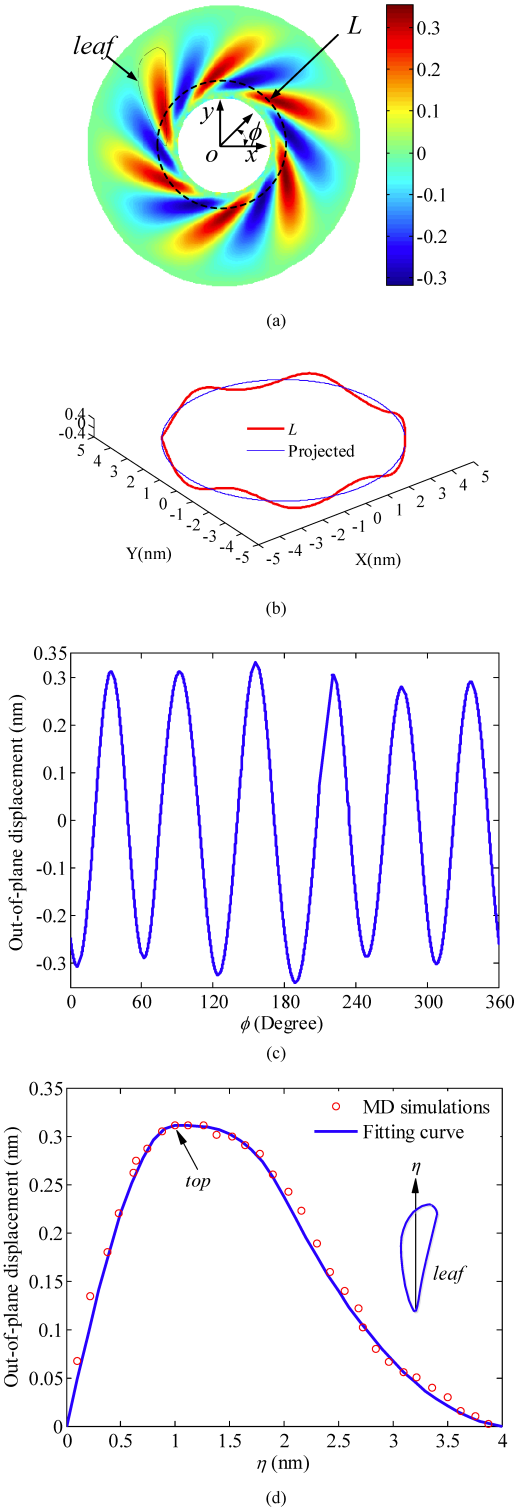

Figure 3. Wrinkle patterns of α-graphyne: (a) wrinkling morphology in terms of out-of-plane displacement (nm) when the rotational angle is 6°; (b) 3D profile of circular lines along with the projected circle on the XY plane; (c) expanded view at the circumferential section "*L*"; (d) wrinkling profile along the longitudinal direction η

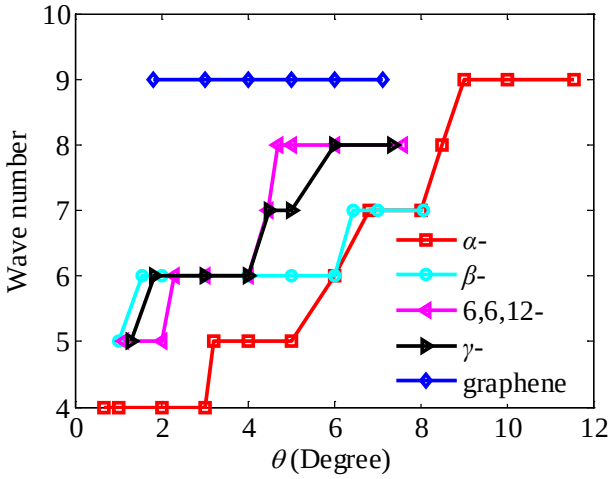

Figure 4. Wave numbers of graphynes and graphene in relation to increasing rotational angles

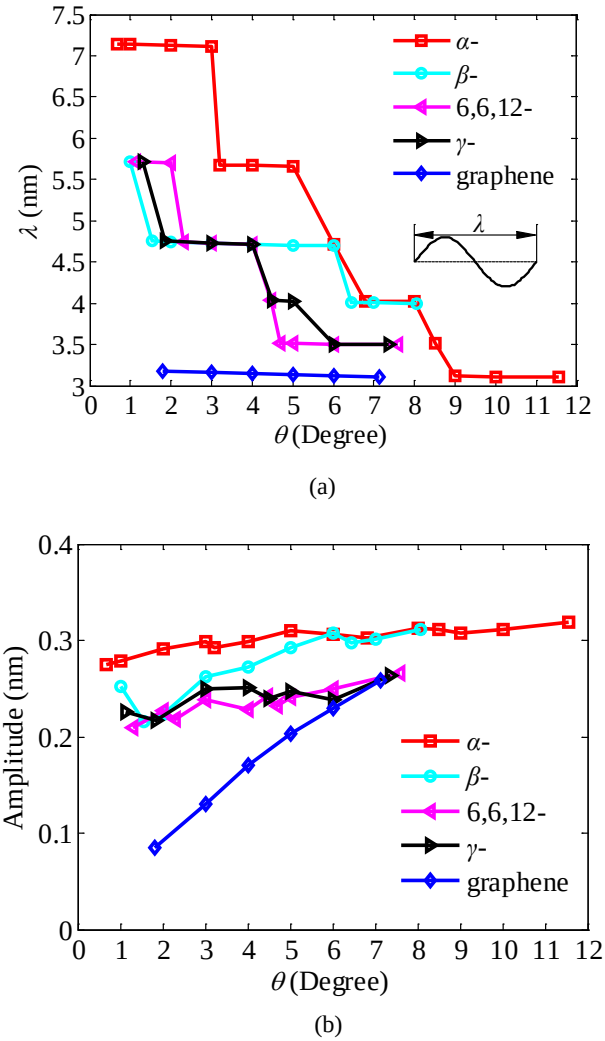

Figure 5. (a) Wavelength and (b) amplitude of graphynes and graphene in relation to increasing rotational angles

show sharp drops, except for that of α-graphyne; there follow a series of small increases and small drops, because the breaking and rearrangement of bonds exist simultaneously. The critical average potential energy of the graphene is higher than for the graphynes. Of the graphynes, α-graphyne has the largest critical average potential energy.

The fractural shearing loads of graphene and β-, 6, 6, 12-, and γ-graphynes are almost the same, while α-graphyne has the largest fracture shearing load. This is mainly due to the higher percentage of acetylenic linkages. The torque of graphene increases linearly with the increasing rotational angles before the initial wrinkling position. After wrinkling generation, the torque retains linearity in relation to the circular shearing load but the slope ratio is slightly reduced. When the rotational angle reaches the fracture point, the torque drops suddenly to a low value. The torque of graphynes linearly changes with the rotational angles and the slope ratio changes at the initial wrinkling positions. However, the slope ratio of graphynes increases after the initial wrinkling angles, which is different to the behaviour of graphene. The fracture torque of graphene is higher than for the graphynes; the fracture torque of α-graphyne is the smallest. The values of the other carbon allotropes β-, 6, 6, 12-, and γ-graphynes are between those of the graphene and α-graphyne, with slight discrepancies among them. The fracture shearing loads show the opposite changes. It can be seen that the fracture shearing loads of graphene and graphynes are correlative with the percentage of acetylenic linkages. The more acetylenic linkages, the higher the fracture shearing load. Since covalently bonded graphynes can be mechanically considered as an atomistic spring-system [17], the elastic constants of sp^1 hybridization are larger than for sp^2 hybridization, and therefore graphynes with a higher percentage of acetylenic linkages have a larger fracture shearing load. That the structural linearity of sp^1 hybridization does not suffer from fluctuation arising from *cis-trans* isomerization [18] may be a further interpretation. Furthermore, the potential energy and torque undergo sharp drops at the fracture rotational angle, except in the case of α-graphyne. The difference stems from the fact that α-graphyne experiences only small structural changes rather than dramatic configuration changes at the fracture point *M*. After the highest torque point *N*, the α-graphyne sheet loses its geometry, such that the dramatic configuration change occurs. A dynamic balance is maintained between torsion energy and bond-breaking energy, so the potential energy of α-graphyne is relatively stable from point *M* to point *N*.

3.4 Bond length

In order to obtain further insights into the mechanical behaviours of such kinds of carbon allotropes, the variations of bond lengths during the wrinkling process were analysed to examine the influences of the acetylenic linkages on the properties of the graphynes. Bond lengths located at points *A*, *B*, *C*, *D* and *E*, as shown in Fig. 1, were chosen for the computational analyses. These bonds are the first to break under the circular shearing loads. The bond-length strain is defined as the relative elongation ratio; the changes in the bond lengths are shown in Fig. 7. We can see that the bond length strains commonly increase with increasing circular shearing loads. Graphene has the larger bond-length strains than any of the graphynes. α- and β-graphynes only have slightly different bond-length strains, both slightly larger than those of γ- and 6, 6, 12- graphynes. The bond-length strains of graphene and α-graphyne quadratically increase approximately with increasing rotational angle, while the other graphynes show an almost linear relationship between the bond-length strains and the shearing loads. The reason is that there are three types of bonds in the graphynes and graphene, i.e., single, double and triple carbon-carbon bonds, and the single bond is not as stiff as the others. Among all the single bonds, those connecting the benzene rings and the acetylene groups are more fragile than others; this is because triple bonds can further weaken adjacent single bonds. This is confirmed by the fracture behaviour of γ- and 6, 6, 12-graphynes, where the bond-breaking occurs at the acetylenic linkages, not the benzene ring. The bonds connecting benzene rings and acetylenic linkages are the most vulnerable in the carbon allotropes, and the fracture generally happens at these positions.

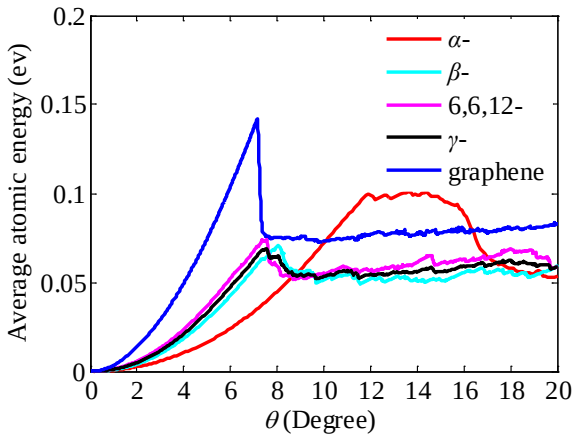

(a)

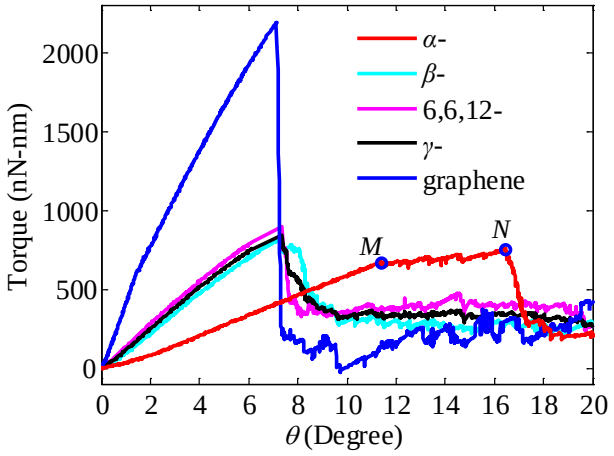

(b)

Figure 6. (a) Average atomic energy and (b) torque of graphynes along with graphene in relation to the rotational angles

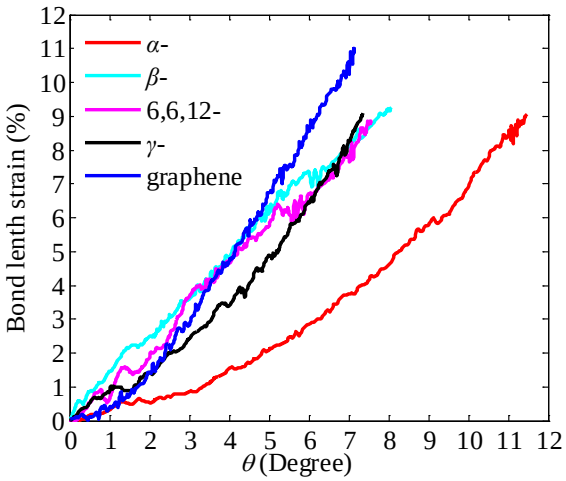

Figure 7. The bond-length strains of graphynes and graphene in relation to rotational angles up to the first bond fracture

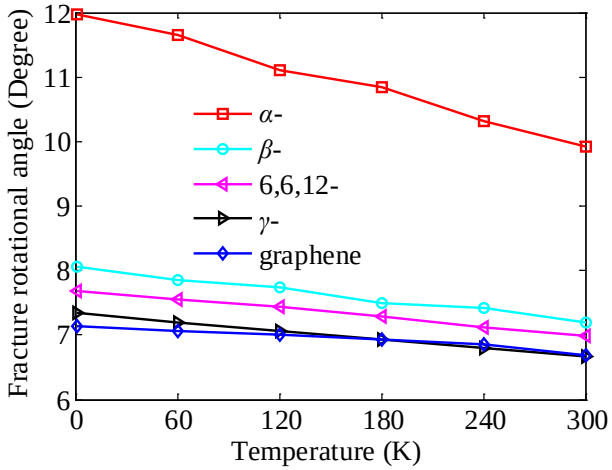

Figure 8. Variations of fracture rotational angles of graphynes and graphene in relation to temperature

3.5 Effect of temperature

It is well known that temperatures have a significant influence on the mechanical properties of carbon-based nanomaterials [41-43]. Thus, it was also necessary to investigate the effects of temperature on the fractural rotational angles of graphene and graphynes for potential applications. The computational conditions were the same as in the previous simulations, with variations only in temperature. Fig. 8 shows the relationship between the fracture rotational angles and temperature. It can be seen that α-graphyne and graphene have the largest and smallest fracture rotational angles at a temperature of 1 K, respectively. The fracture rotational angles of the other graphynes are located between the extreme values. By increasing the temperature up to 300 K, the fracture rotational angle is decreased, approximately linearly. The decline rate of graphene is lower than for γ-graphyne, and thus the two corresponding curves cross over at the temperature of 180 K. The fracture rotational angle of α-graphyne decreases from 11.7° to 9.6°, reducing by a ratio of 17.9%. The graphene shows fracture rotational angle reduction from 7.1° to 6.8°, corresponding to a decrease ratio of 4.2%. β-, γ- and 6, 6, 12-graphynes have almost the same decrease ratio of 5.5%. This indicates that the temperature changes have a significant influence on the acetylenic linkages. The increased temperatures enlarge the thermal vibration of the atoms and thus increase the thermal energy, which reduces the fracture strain energy for the carbon allotropes.

4. Conclusions

The wrinkling behaviours of annular graphynes under circular shearing load at the inner edge have been investigated utilizing classic molecular-dynamics simulations. The generation and development of wrinkling patterns on the graphynes have been explored to obtain keys to enabling techniques for potential applications. It was found that the graphynes have a sinusoidal profile at the circumference located at the maximum crest. Wrinkling-profile characterization in terms of wave number, wavelength and amplitude was conducted, and it was demonstrated that the wave number of graphene remains constant in the special outer-to-inner radius ratio during the wrinkling process, while that of the graphynes increases with the increasing rotational angles.

The average potential energy and torque of such kinds of carbon allotropes have also been explored to obtain further insights into the mechanical properties of graphynes. It has been established that the introduction of acetylenic linkages will generally reduce the fractural potential energy of graphynes. The more acetylenic linkages there are, the larger the reduction in the fracture potential energy. The influence of acetylenic linkages on fractural torque is the same as for fractural potential energy. The bond-length change ratios of the graphynes during the wrinkling process are also related to the percentages of acetylenic linkages. It has been demonstrated that graphene has a greater bond-length ratio than any of the graphynes. The bond-breaking commonly occurred at the connection between the acetylenic linkage and the benzene ring. Increased temperature generally reduced the fractural rotational angles, and the fractural rotational angle reduction of graphene was smaller than for graphynes. This indicates that the acetylenic linkages are more sensitive to temperature changes. The achieved research results contribute to advanced knowledge of graphynes for their potential application.

5. Acknowledgements

This research was supported by the National Natural Science Foundation of China (No. 51175372), the Reserved Academic Programme of Peiyang Scholar, and the Programme for New Century Excellent Talents in University (No. NCET -11-0374).

6. References

[1] Zhang J W, Jiang D Z (2014) Molecular Dynamics Simulations of Mechanical Performance of Graphene/Graphene Oxide Paper Based Polymer Composites. Carbon 67: 784-791.

[2] Li Y F, Datta D, Li Z H et al (2014) Mechanical Properties of Hydrogen Functionalized Graphene Allotropes. Computational Materials Science 83: 212-216.

[3] Yi L J, Yin Z N, Zhang Y Y et al (2013) A Theoretical Evaluation of the Temperature and Strain-Rate Dependent Fracture Strength of Tilt Grain Boundaries in Graphene. Carbon 51: 373-380.

[4] Han J H, Ryu S H, Sohn D W et al (2014) Mechanical Strength Characteristics of Asymmetric Tilt Grain Boundaries in Graphene. Carbon 68: 250-257.

[5] Baughman R H, Eckhardt H, Kertesz M (1987) Structure Property Predictions for New Planar Forms of Carbon: Layered Phases Containing Sp^2 and *Sp* Atoms. Journal of Chemical Physics 87: 6687-6699.

[6] Haley M M, Brand S C, Pak J J et al (1997) Carbon Networks Based on Dehydrobenzoannulenes: Synthesis of Graphdiyne Substructures, Angewandte Chemie. International Edition in English 36, No 8: 836-838.

[7] Diederich F, Kivala M (2010) All-Carbon Scaffolds by Rational Design. Advanced Materials 22: 803-812.

[8] Li G X, Li Y L, Liu H B et al (2010) Architecture of Graphyne Nanoscale Films. Chemical Communications 46: 3256-3258.

[9] Ivanovskii A L (2013) Graphynes and Graphyines. Progress in Solid State Chemistry 42: 1-19.

[10] Malko D, Neiss C, Vines F, Gorling A (2012) Competition For Graphene: Graphynes With Direction-Dependent Dirac Cones. Physical Review Letters 108: 086804(6p).

[11] Jing Y H, Wu G X, Guo L C, et al (2013) Electronic Properties of Graphyne and Its Family. Computational Materials Science 78: 22-28.

[12] Yang Y L, Xu X M (2012) Mechanical Properties of Graphyne and Its Family – A Molecular Dynamics Investigation. Computational Materials Science 61: 83-88.

[13] Pei Y (2012) Mechanical Properties of Graphdiyne Sheet. Physica B: Condensed Matter 407: 4436-4439.

[14] Pan L D, Zhang L Z et al (2011) Graphyne- and Graphiyne-Based Nanoribbons: Density Functional Theory Calculations of Electronic Structures. Applied Physics Letters 98: 173102(4p).

[15] Haley M M (2008) Synthesis and Properties of Annulenic Subunits of Graphyne and Graphdiyne Nanoarchitectures. Pure and Applied Chemistry 80: 519-532.

[16] Ni Y, Yao K L, Fu H H, et al (2013) The Transport Properties and New Device Design: the Case of 6, 6, 12-Graphyne Nanoribbons. Nanoscale 5: 4468-4475.

[17] Cranford S W, Buehler M J (2011) Mechanical Properties of Graphyne. Carbon 49: 4111-4121.

[18] Salmalian K, Rouhi S, Mehran S (2015) Molecular Dynamics Simulations of the Buckling of Graphyne and Its Family. Physica B: Condensed Matter 457: 135-139.

[19] Shao T J, Wen B, Melnik R, et al (2012) Temperature Dependent Elastic Constants and Ultimate Strength of Graphene and Graphyne. The Journal of Chemical Physics 137: 194901(30p).

[20] Zhang Y Y, Pei Q X, Wang C M et al (2013) A Molecular Dynamics Investigation on Mechanical Properties of Hydrogenated Graphynes. Journal of Applied Physics 114: 073504(7p).

[21] Majidi R, Karami A R (2014) Adsorption of Formaldehyde On Graphene and Graphyne. Physica E: Low-Dimensional Systems and Nanostructures 59: 169-173.

[22] Ning G Q, Xu C G, Zhu X et al (2013) Mgo-Catalyzed Growth of N-Doped Wrinkled Carbon Nanotubes. Carbon 56: 38-44.

[23] Mei Y F, Kiravittaya S, Harazim S et al (2010) Principle and Applications of Micro and Nanoscale Wrinkles. Materials Science and Engineering: R: Reports 70: 209-224.

[24] Duan W H, Gong K, Wang Q (2011) Controlling of Formation of Wrinkles in a Single Layer Graphene Sheet Subjected to in-Plane Shear. Carbon 49: 3107-3112.

[25] Calado V E, Schneider G F, Theulings A M M G et al (2012) Formation and Control of Wrinkles in Graphene by the Wedging Transfer Method. Applied Physics Letters 101: 103116(3p).

[26] Bai S, Shen X P, Zhu G X et al (2013) the Influence of Wrinkling in Reduced Graphene Oxide On Their Adsorption and Catalytic Properties. Carbon 60: 157-168.

[27] Tian Y, Li Z, Gao W et al (2014) Mechanical Properties Investigation of Monolayer H-BN Sheet Under in-Plane Shear Displacement Using Dynamics Simulations. Journal of Applied Physics 115: 014308(9p).

[28] Zhang Y Y, Peng Q X, Wang C M (2012) Mechanical Properties of Graphynes under Tension: A Molecular Dynamics Study. Applied Physics Letters 101: 081909(7p).

[29] Stuart S J, Tutein A B, Harrison J A (2010) A Reactive Potential for Hydrocarbons with Intermolecular Interactions. The Journal of Chemical Physics 112: 6472-6486.

[30] Brenner D W, Shenderova O A, Harrison J A et al (2002) A Second-Generation Reactive Empirical

Bond Order (REBO) Potential Energy Expression of Hydrocarbons. Journal of Physics: Condensed Matter 14: 783-802.

[31] Hur J, Stuart S J (2012) Modified Reactive Empirical Bond-Order Potential For Heterogeneous Bonding Environments. Journal of Chemical Physics 137: 0504102(8p).

[32] Wei N, Xu L Q, Wang H Q et al (2011) Strain Engineering of thermal Conductivity in Graphene Sheets and Nanoribbons: A Demonstration of Magic Flexibility. Nanotechnology 22: 105705(11p).

[33] Pei Q X, Zhang Y W, Shenoy V B (2010) A Molecular Dynamics Study of the Mechanical Properties of Hydrogen Functionalized Graphene. Carbon 48: 898-904.

[34] Shenderova O A, Brenner D W (2000) Atomistic Modeling of the Fracture of Polycrystalline Diamond. Physical Review B 61: 3877-3888.

[35] Hoover W G (1985) Canonical Dynamics: Equilibrium Phase-Space Distributions. Physical Review A 31: 1695-1697.

[36] Allen M P, Tildeseley D J (1987) Computer Simulation of Liquids. Oxford: Clarendon Press.

[37] Zhang C L, Shen H S (2008) Predicting the Elastic Properties of Double-Walled Carbon Nanotubes by Molecular Dynamics Simulation. Journal of Physics D: Applied Physics 41: 055404(6p).

[38] Zhang Z, Duan W H, Wang C M (2013) A Grillage Model For Predicting Wrinkles in Annular Graphene Under Circular Shearing. Journal of Applied Physics 113: 014902(7p).

[39] Zhang Z, Duan W H, Wang C M (2012) Tunable Wrinkling Pattern in Annular Graphene Under Circular Shearing At inner Edge. Nanoscale 4, No 16: 5077-5081.

[40] Ducere J M, Lepetit C, and Chauvin R (2013) Carbon-Graphite: Structural, Mechanical and Electronic Properties. The Journal of Chemical Physics C 117: 21671-21681.

[41] Vijayaraghavan V, Wong C H (2013) Temperature, Defect and Size Effect on the Elastic Properties of Imperfectly Straight Carbon Nanotubes by Using Molecular Dynamics Simulation. Computational Materials Science 71: 184-191.

[42] Dewapriya M, Srikantha A (2013) influence of Temperature and Free Edges On the Mechanical Properties of Graphene. Modelling and Simulation in Materials Science and Engineering 21: 065017(15p).

[43] Shao T, Wen B, Melnik R et al (2012) Temperature Dependent Elastic Constant and Ultimate Strength of Graphene and Graphyne. The Journal of Chemical Physics 139: 194901(8p).